13TH CANADIAN MASONRY SYMPOSIUM
HALIFAX, CANADA
JUNE 4TH – JUNE 7TH 2017

NONLINEAR FINITE ELEMENT MODELLING OF UNREINFORCED MASONRY WALLS WITH OPENINGS SUBJECTED TO IN-PLANE SHEAR

Allen, Clive[1]; Masia, Mark[2]; Page, Adrian[3]; Griffith, Michael[4] and Ingham, Jason[5]

ABSTRACT

This paper presents a numerical investigation into the behaviour of unreinforced clay brick masonry walls with window and door type openings, subjected to in-plane loads. Nonlinear finite element simulations of full scale walls experimentally tested at The University of Newcastle have been undertaken using the commercial finite element analysis software TNO DIANA. In this study, both continuum (total strain fixed-crack) and simplified micro-model (crack-shear-crush) nonlinear finite element modelling strategies have been employed and key parameters including force versus displacement curves, failure modes, and damage patterns have been compared to experimental results.

KEYWORDS: *unreinforced masonry, seismic loading, numerical analysis*

INTRODUCTION

Unreinforced masonry buildings and earthquakes

The seismic vulnerability of unreinforced masonry (URM) buildings has consistently been demonstrated in recent earthquakes such as Newcastle 1989, L'Aquila 2009, Haiti 2010, Christchurch 2010-2011, and Nepal 2015. Observations from previous earthquakes have shown that damage to URM walls due to in-plane seismic loading is common, but structural collapse of buildings due to in-plane actions usually only occurs in walls with openings [1].

[1] PhD Student, Centre for Infrastructure Performance and Reliability, The University of Newcastle, University Drive, Callaghan, NSW 2308, Australia, clive.k.allen@gmail.com
[2] Associate Professor, Centre for Infrastructure Performance and Reliability, The University of Newcastle, University Drive, Callaghan, NSW 2308, Australia, mark.masia@newcastle.edu.au
[3] Emeritus Professor, Centre for Infrastructure Performance and Reliability, The University of Newcastle, University Drive, Callaghan, NSW 2308, Australia, adrian.page@newcastle.edu.au
[4] Professor, School of Civil, Environmental and Mining Engineering, The University of Adelaide, Engineering North N136, North Terrace Campus, SA 5005, Australia, michael.griffith@adelaide.edu.au
[5] Professor, Department of Civil and Environmental Engineering, University of Auckland, Newmarket Campus, B906-237, Auckland 1023, New Zealand, j.ingham@auckland.ac.nz

Numerical modelling of unreinforced masonry

Various strategies exist for the numerical modelling of unreinforced masonry. The four most common analysis types are, in increasing order of complexity: Linear static, linear dynamic, nonlinear static, and nonlinear dynamic analysis. Due to the highly nonlinear behaviour of the URM material when subjected to seismic loading, linear methods are not always suitable for the seismic analysis of URM walls. Due to the high complexity of nonlinear dynamic analysis, considerable computation time and operator skill is required in order to achieve reasonable results. Therefore, the nonlinear static (pushover) analysis method for URM walls is gaining popularity with both consulting engineers and academia. Previous Australian studies such as [2] and [3] have simulated the results of experimentally tested solid walls subject to in-plane loads, and authors such as [4] have used simplified nonlinear finite element models to replicate walls representative of New Zealand construction with openings subject to in-plane loads, but to the authors' knowledge, there has been no previous nonlinear finite element modelling of walls representative of Australian URM construction with openings.

EXPERIMENTAL TESTS OF IN-PLANE WALLS

Full details of the wall testing programme used as the basis for the finite element analysis (FEA) study presented in this paper are presented in [5]. A brief summary of the results is provided alongside the FEA results presented in Figure 4 through Figure 12.

Wall Geometry

The experimental testing programme consisted of three different wall geometry types which are presented in Figure 1. These wall geometric characteristics were determined based on typical unreinforced masonry wall typologies observed in existing Australian construction, and were selected so that distinct failure modes would be observed between the three wall geometries. The walls were constructed of a single skin of clay brick units measuring 230mm × 110mm × 76mm. A 100mm × 100mm × 10mm equal angle section lintel was used to support the masonry over wall openings for all walls.

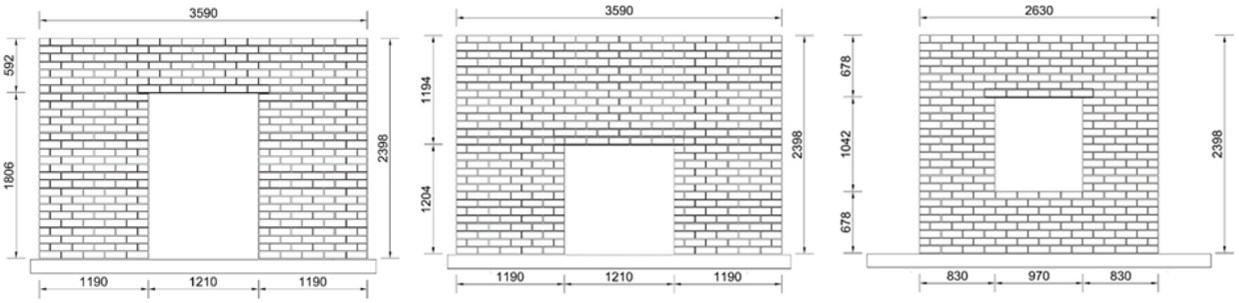

a) Wall type W01 **b) Wall type W02** **c) Wall type W03**

Figure 1: Wall geometrical characteristics

Experimental Test Setup

The experimental testing setup is shown in Figure 2 and consisted of a vertical load applied to the centreline of each of the wall piers which was applied via a jack reacting against a strong beam /

strong wall setup and a spreader beam which allowed the load to be evenly distributed to each of the wall piers. Cyclic lateral displacements of increasing amplitude were applied to the wall via a horizontal jack reacting against a strong wall. This horizontal jack was connected with two jack extension arms to a loading beam which was glued to the top of the unreinforced masonry walls.

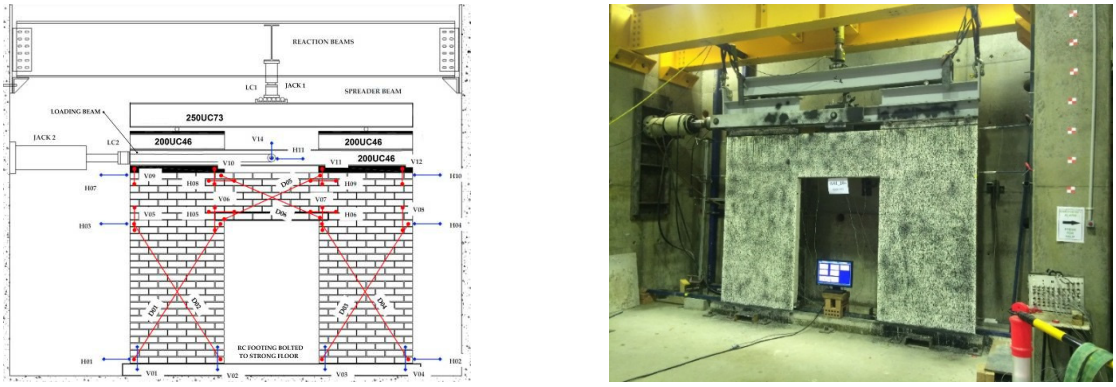

a) Elevation of test setup. Wall type W01 shown.

b) As-built test setup for wall W01_10a

Figure 2: Experimental test setup

Wall Test Matrix

The walls tested in the experimental programme modelled in this study consisted of three geometrical types (W01, W02, W03), two precompression levels (0.2MPa and 1.0MPa) and two repeats (a,b), giving a total of 12 wall tests undertaken. The wall labelling convention is as follows: <wall geometry>_<wall precompression>_<test repeat>. A summary of the walls tested is presented in Table 1.

Table 1: Wall test matrix

Geometry	Precompression	Wall test ID	
W01	0.2 MPa	W01_02a*	W01_02b
W01	1.0 MPa	W01_10a*	W01_10b
W02	0.2 MPa	W02_02a*	W02_02b
W02	1.0 MPa	W02_10a	W02_10b*
W03	0.2 MPa	W03_02a	W03_02b*
W03	1.0 MPa	W03_10a*	W03_10b

*Denotes wall test digital image correlation output used in Figure 4 through Figure 9.

Measured material properties

During the experimental programme, several material parameters were measured in order to characterise the as-built properties of the walls. The main control parameter for the walls tested was the flexural bond strength of masonry. For every batch of mortar used in the construction of the 12 walls (2-3 batches used per wall), 10 mortar joints were tested using a bond-wrench test and the masonry flexural bond strength was determined based on these results. A weak cementitious (1:1:6 cement:lime:sand by volume) mortar with a bond strength of approximately 0.15 MPa was targeted for the experimental programme in order to be representative of typical existing Australian URM construction, and to give a range of failure modes. Masonry compressive strength, Masonry

elastic modulus, brick tensile strength, mortar joint cohesion and mortar joint friction coefficients were determined from tests undertaken only once in the wall testing programme, due to the increased level of time and resources required to undertake these tests. A summary of the average values of these material parameters is contained in Table 2.

Table 2: Summary of average measured masonry material parameters for walls tested

Parameter		Average	Test method
Masonry compressive strength	f_m	9.64 MPa	Prism compression test [6]
Masonry elastic modulus	E_m	9573 MPa	Prism compression test [6]
Mortar flexural bond strength	f_{mt}	0.16 MPa	Bond-wrench test [6]
Tensile strength of brick	$f_{ut} = f_{ct,f} / 1.5$	1.93 MPa	Lateral modulus of rupture test [7]
Cohesion of mortar joint	c	0.46 MPa	Triplet test [8]
Friction coefficient of mortar	$\mu_f = \tan[\varphi]$	0.83	Triplet test [8]

Summary of key experimental test results

The experimentally tested walls failed in a mixture of pier and spandrel flexural and shear modes depending on the wall geometry and vertical precompression level. Cracking generally occurred through the masonry bed and head joints rather than the brick units, which is to be expected given the relatively weak mortar strength. W01_02 and W03_02 series of tests typically exhibited flexural modes of damage in the piers, with spandrel damage due to bed-joint sliding only occurring at the very end stages of the test. W01_10 and W03_10 series of tests exhibited similar damage in the piers to W01_02 and W03_02, but with spandrel bed-joint sliding and stepped shear cracking observed earlier in the loading regime. Wall W02_02a exhibited rocking type behaviour of piers followed by diagonal shear cracking of the left hand pier resulting in a rapid loss of strength. W02_02b exhibited the same rocking type behaviour at the early stages of the test, but the test was stopped before any shear crack could develop in the piers, due to the debonding of the top beam of the test setup. W02_10 exhibited combined diagonal shear cracking of the spandrel and rocking of piers for both repeats of the test. Digital image correlation (DIC) results of the tests nominated by * in Table 1 are presented in Figure 4 through Figure 9 for the positive (left hand) direction of loading. Envelopes of the experimentally recorded load vs. lateral displacement of loading beam are presented in Figure 10 through Figure 12.

NONLINEAR FINITE ELEMENT MODELLING METHODOLOGY

For this study, two finite element modelling strategies were undertaken; micromodelling and macromodelling. The micromodel approach used the crack-shear-crush model, where the wall is modelled as a series of linearly elastic expanded half brick units with interface elements representing mortar joints and possible brick crack locations. The macromodelling approach makes the approximation of masonry as a continuous, homogenous medium with smeared mechanical properties. A schematic representation of each of these modelling strategies is shown in Figure 3. The commercial finite element package TNO DIANA [9] was used for all finite element modelling work presented in this study. For both micro and macromodelling approaches, a vertical load was applied to the centreline of the wall piers via the steel loading beams and then a displacement was incrementally applied at the top midspan of the loading beam. This displacement was applied monotonically in increments of between 0.05mm and 1mm, depending

on wall geometry and convergence of the model. Finite element models were generally run until the model ceased to converge, or the maximum displacement of the experimental test for the corresponding wall was reached.

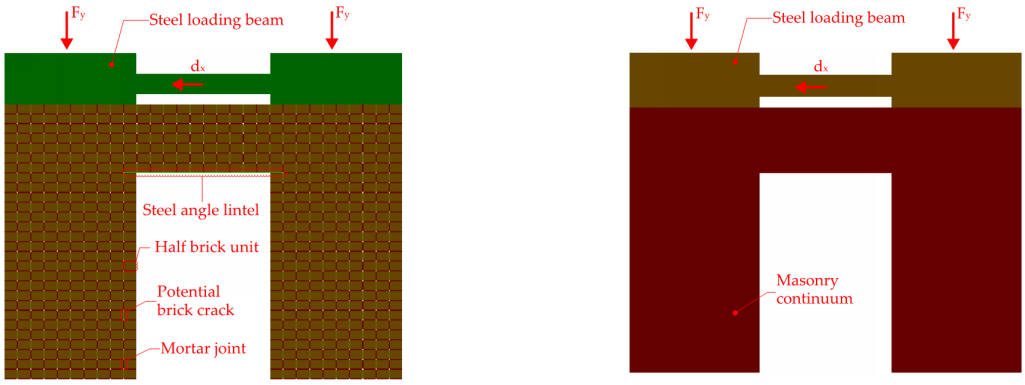

a) Micromodel **b) Macromodel**

Figure 3: Finite element model overview (wall geometry type W01 shown)

Finite Element Model Input Parameters

Input parameters for both the micro and macromodels were determined based on the measured material properties contained in Table 2, and previous numerical and experimental studies. Summaries of key input parameters for both modelling strategies are presented in Table 3 and Table 4 respectively.

Table 3: Summary of key masonry material parameters for finite element micro model

Parameter		Adopted value	Comments
Elastic modulus of brick units	E_{unit}	21788 MPa	Determined by test
Elastic modulus of mortar joint	E_{mor}	1933 MPa	Determined by test
Poisson's ratio of brick units	ν	0.20	Assumed
Normal stiffness of brick unit	k_n	1×10^6 N/mm	[10]
Shear stiffness of brick unit	k_s	1×10^6 N/mm	[10]
Tensile strength of brick unit	f_t	1.93 MPa	Determined by test
Tensile fracture energy of mortar joint	G^I_f	0.056 N/mm	[11]
Normal stiffness of mortar joint	k_n	212 N/mm	[10]
Shear stiffness of mortar joint	k_s	88 N/mm	[10]
Tensile strength of mortar joint	f_t	0.11 MPa	
Tensile fracture energy of mortar joint	G^I_f	0.003 N/mm	[11]
Cohesion of mortar joint	c_0	0.40 MPa	Determined by test*
Initial friction coefficient of mortar joint	$\tan[\phi_i]$	0.83	Determined by test
Initial dilatancy coefficient of mortar joint	$\tan[\psi_0]]$	0.50	[2]
Residual friction coefficient of mortar joint	$\tan[\phi_r]$	0.56	[2]
Confining normal stress for zero initial dilatancy	σ_u	-0.75	[2]
Dilatancy shear-slip degradation coeffcient	δ	1.8	[2]
Compressive strength of masonry	f_m	9.64 MPa	Determined by test
Masonry fracture energy in compression	G_c	15.42 N/mm	[11]
Shear traction contribution factor	C_s	9.0	[10]
Equivalent plastic relative displacement	κ_p	0.015	[10]
Mode II fracture energy coefficient (a)	$G^{II}_f(a)$	-0.80	[2]
Mode II fracture energy coefficient (b)	$G^{II}_f(b)$	0.05	[2]

*cohesion value limited to 0.40MPa in order to satisfy input parameter requirements for crack-shear-crush model.

Table 4: Summary of key masonry material parameters for finite element macro model

Parameter		Adopted value	Comments
Masonry elastic modulus	E_m	9573 MPa	Determined by test
Masonry Poisson's ratio	ν	0.2	Assumed
Masonry tensile strength	$f_t \approx f_m/20$	0.48 MPa	[11]
Masonry tensile fracture energy	G_t	0.05 N/mm	Assumed
Masonry compressive strength	f_m	9.64 MPa	Determined by test
Masonry compressive fracture energy	G_t	15.42 N/mm	[11]
Masonry shear retention factor	β	0.05	Assumed
Masonry crack bandwidth	-	$(A)^{1/2}$	DIANA default

NONLINEAR FINITE ELEMENT MODELLING RESULTS

Experimental and Finite Element Analysis crack patterns

Crack patterns at the ultimate limit state for the walls tested experimentally, simulated using micro FEA, and macro FEA are presented in Figure 4 through Figure 9 a), b), and c) respectively. Note that the experimental data presented in these figures shows measured principal strain contours as a measure of damage. The micromodel data presented in these figures shows relative crack size. The macromodel data presented in these figures shows principal strain contours. For all output data in Figure 4 through Figure 9, red contours are indicative of increasing crack magnitude.

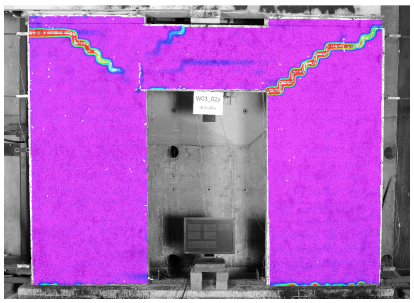

a) Experimental d = 28mm (1.17%)

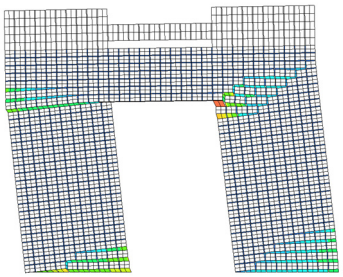

b) Micromodel d=15mm (0.63%)

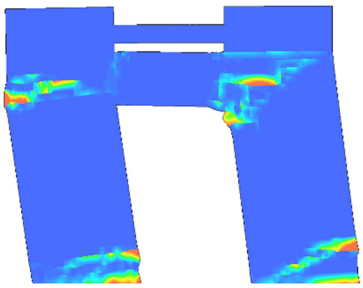

c) Macromodel d=15mm (0.63%)

Figure 4: W01_02 damage patterns from experimental and FEA analyses

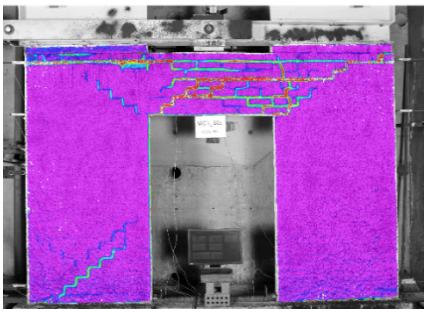

a) Experimental d = 28mm (1.17%)

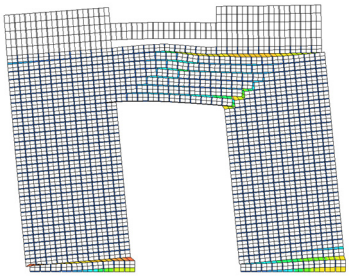

b) Micromodel d=15mm (0.63%)

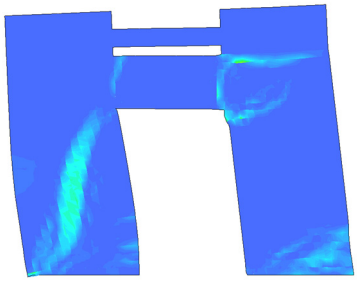

c) Macromodel d=15mm (0.63%)

Figure 5: W01_10 damage patterns from experimental and FEA analyses

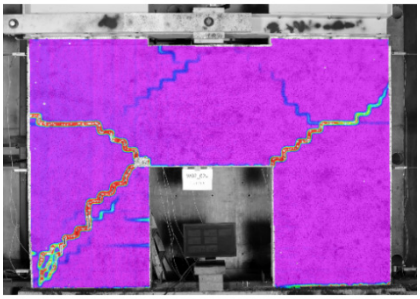

a) Experimental d = 10mm (0.42%)

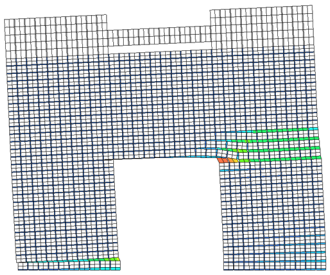

b) Micromodel d=8mm (0.33%)

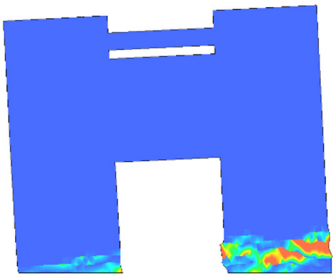

c) Macromodel d=8mm (0.33%)

Figure 6: W02_02 damage patterns from experimental and FEA analyses

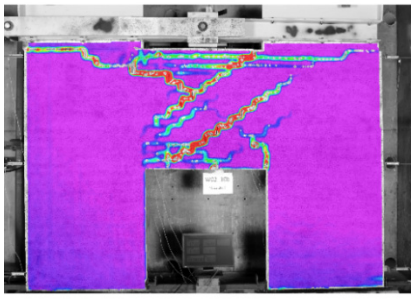

a) Experimental d = 18mm (0.75%)

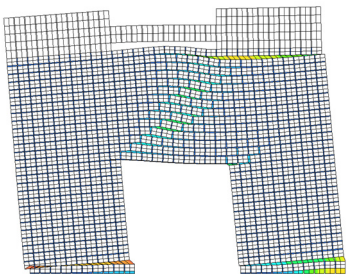

b) Micromodel d=15mm (0.63%)

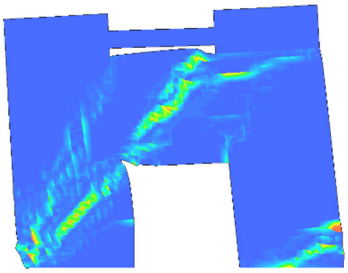

c) Macromodel d=15mm (0.63%)

Figure 7: W02_10 damage patterns from experimental and FEA analyses

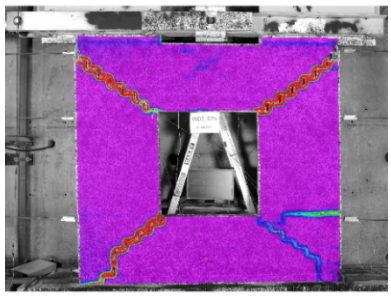

a) Experimental d = 22mm (0.92%)

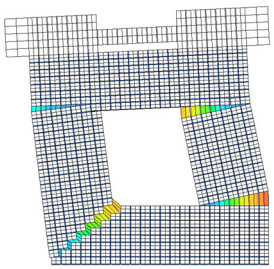

b) Micromodel d=15mm (0.63%)

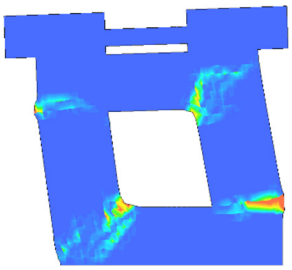

c) Macromodel d=15mm (0.63%)

Figure 8: W03_02 damage patterns from experimental and FEA analyses

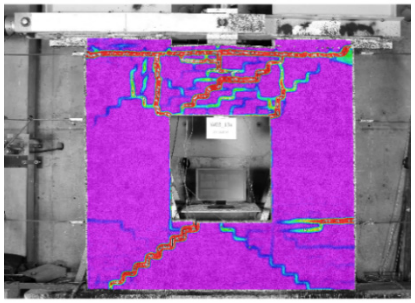

a) Experimental d = 28mm (1.17%)

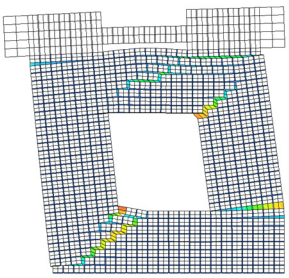

b) Micromodel d=15mm (0.63%)

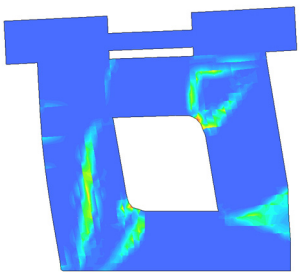

c) Macromodel d=15mm (0.63%)

Figure 9: W03_10 damage patterns from experimental and FEA analyses

Experimental and Finite Element Analysis Force-Displacement Relationships

The force-displacement relationships for the walls experimentally tested were compared with the force-displacement relationships predicted by the micro and macro FEA models. A summary of this information is presented in Figure 10 through Figure 12. Note that all 12 walls experimentally tested are included in this comparison and are presented as envelope curves of force-displacement hysteresis curves.

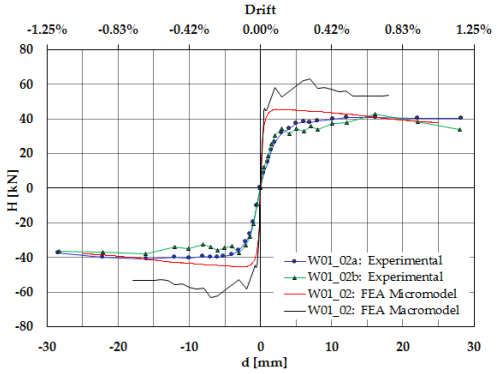

a) W01_02

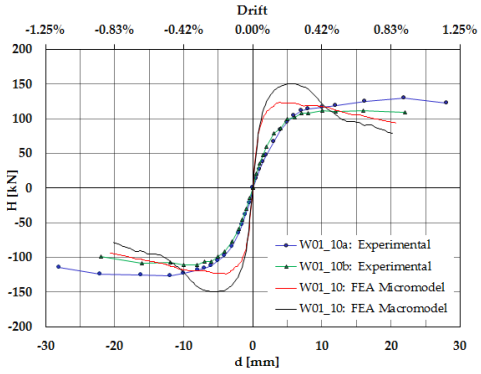

b) W01_10

Figure 10: Force displacement graphs of experimental and FEA results for W01

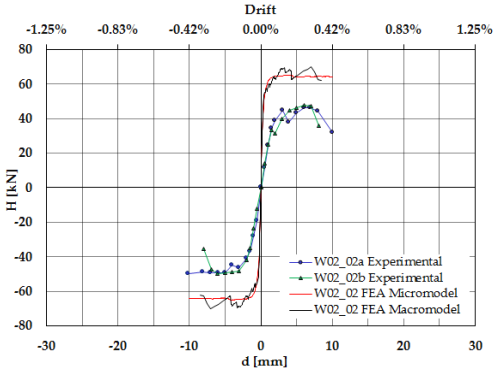

a) W02_02

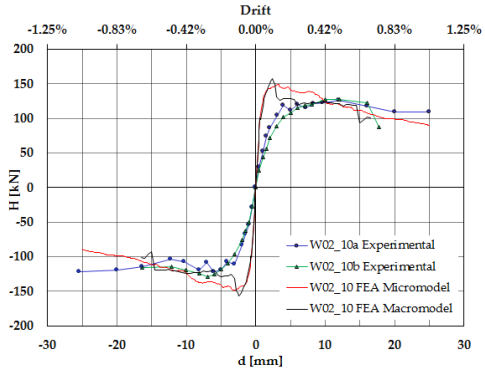

a) W02_10

Figure 11: Force displacement graphs of experimental and FEA results for W02

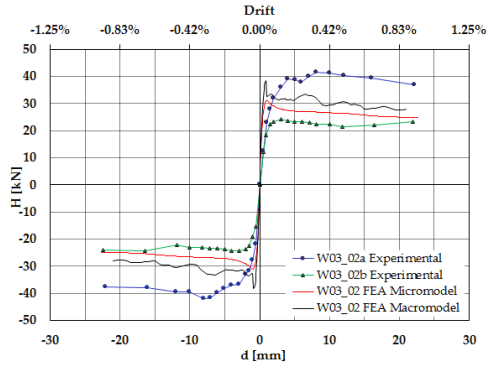

a) W03_02

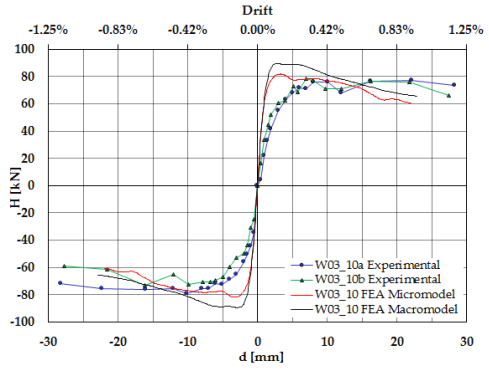

b) W03_10

Figure 12: Force displacement graphs of experimental and FEA results for W03

Experimental and Finite Element Analysis bilinear wall response parameters

Based on the results of the Micromodel and Macromodel finite element analyses, bilinear in-plane wall response parameters were determined using the method outlined in [12]. A summary of these response parameters is presented in Table 5, and a graphical description of this procedure is shown in Figure 13.

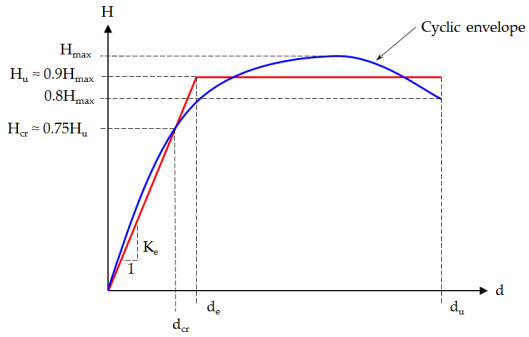

Figure 13: Bilinear response parameter definition (adapted from [12])

Table 5: Summary of bilinear wall response parameters

	H_u	d_e	Δ_e	d_u	Δ_u	μ	K_e	$H_{u.FEA}/H_{u.EXP}$	μ_{FEA}/μ_{EXP}	$K_{e.FEA}/K_{e.EXP}$
	[kN]	[mm]	[%]	[mm]	[%]	[-]	[N/mm]	[-]	[-]	[-]
W01_02 Micro*	41	0.4	0.02%	25.0	1.04%	62.5	102	1.12	5.2	6.54
W01_02 Macro**	57	0.5	0.02%	18.0	0.75%	33.8	106	1.55	2.8	6.79
W01_02 Exp***	37	2.4	0.10%	28.2	1.18%	12.1	16	-	-	-
W01_10 Micro	112	1.2	0.05%	17.8	0.74%	14.8	93	1.03	2.6	3.80
W01_10 Macro	135	1.6	0.07%	10.2	0.43%	6.4	84	1.25	1.1	3.45
W01_10 Exp	108	4.4	0.19%	25.0	1.04%	5.6	24	-	-	-
W02_02 Micro	59	0.4	0.02%	10.0	0.42%	25.0	146	1.34	5.3	6.21
W02_02 Macro	63	0.4	0.02%	8.5	0.35%	21.3	158	1.45	4.5	6.70
W02_02 Exp	44	1.9	0.08%	8.7	0.36%	4.7	24	-	-	-
W02_10 Micro	134	0.9	0.04%	12.2	0.51%	14.1	155	1.18	2.0	4.16
W02_10 Macro	141	1.1	0.04%	10.0	0.42%	9.4	132	1.25	1.3	3.57
W02_10 Exp	113	3.1	0.13%	20.9	0.87%	7.1	37	-	-	-
W03_02 Micro	28	0.4	0.02%	22.7	0.95%	56.8	70	0.94	3.1	3.11
W03_02 Macro	35	0.4	0.02%	12.0	0.50%	30.0	86	1.16	1.7	3.85
W03_02 Exp	30	1.3	0.06%	22.1	0.92%	18.1	22	-	-	-
W03_10 Micro	74	1.1	0.04%	17.0	0.71%	15.9	69	1.07	1.6	2.81
W03_10 Macro	80	1.2	0.05%	16.7	0.70%	13.9	67	1.16	1.4	2.73
W03_10 Exp	69	2.8	0.12%	27.9	1.16%	9.9	25	-	-	-

*Micro denotes: FEA micromodel

**Macro denotes: FEA macromodel

***Exp denotes: Experimental results. Note that the experimental results listed in the table above are the averages of the positive and negative directions of both repeats of the wall, that is, the average of 4 values for each parameter.

Where:
H_u is the ultimate strength of the wall,
d_u, d_e are the ultimate and equivalent bilinearised yield displacements of the wall, respectively
Δ_u, Δ_e are the ultimate and equivalent bilinearised yield drifts of the wall, respectively
$K_e = H_u/d_e$ is the initial elastic stiffness of the wall
$\mu = d_u/d_e = \Delta_u/\Delta_e$ is the structural ductility factor

DISCUSSION OF RESULTS

The failure modes and crack patterns predicted by the nonlinear finite element analyses were generally in good agreement with those obtained by the experimental programme. For wall W02_02, both micro and macro models did not capture the failure mode of diagonal stepped cracking through mortar joints of the left hand side pier, thus over estimating the ultimate strength and displacement capacity of the wall. Further investigation of the variability of material properties within each wall is required in order to capture this failure mode.

Generally the micro models provided a better representation of the failure mode and load than the macro model. This is to be expected, due to the explicit representation of masonry units and mortar for the micro model. The force vs. displacement behaviour obtained from the nonlinear finite element analyses were in reasonable agreement with those obtained by the experimental programme. It was clear however that the predicted initial stiffness of the walls was far in excess of that measured experimentally. Both micro and macro models did not accurately capture the initial elastic stiffness of the walls experimentally tested, with the initial stiffness predicted by the FEA analyses ranging from 2.73 – 6.46 times the experimentally tested initial stiffness. Possible reasons for this discrepancy in initial stiffness include the anisotropy of perforated clay brick units, and the fact that the elastic modulus of masonry prisms is measured in compression only, and gives little information regarding the stiffness of masonry in tension, which up until the point of cracking is assumed to be equal to the stiffness in compression. For walls with low precompression levels this assumption can be a significant source of error.

CONCLUSIONS AND FURTHER WORK

Conclusions

- Nonlinear FEA gives a good estimate of peak loads and failure modes.
- Information regarding initial stiffness and ductility did not match experimental observation – further work is required in order to properly characterise the initial stiffness of the wall.
- Micromodel FEA provides better replication of experimental results than macromodel.

Further work

- Sensitivity analysis with respect to wall inelastic and elastic parameters is required in order to determine suitable input parameters for macro models.
- Extension of finite element macro modelling to include walls tested in Auckland [4].

ACKNOWLEDGEMENTS

The authors graciously acknowledge the financial support provided by the Australian Research Council under Discovery Project DP120100848. The authors would like to thank to Brickworks Building Products for their generous donation of materials for the experimental testing programme. The authors also extend their gratitude to the civil engineering laboratory staff at The University of Newcastle; Andy, Goran, Ian, Ross and Mick for their patience and expertise.

REFERENCES

[1] Ingham, J. M. & Griffith, M. C. (2011). "The performance of unreinforced masonry buildings in the 2010/2011 Canterbury earthquake swarm. Canterbury Earthquakes Royal Commission of Inquiry, Christchurch, New Zealand.

[2] Petersen, R. B. (2009). "In-plane shear behaviour of unreinforced masonry panels strengthened with fibre reinforced polymer strips." PhD thesis, University of Newcastle, Australia.

[3] Konthesingha, K. M. C. (2012). "Earthquake protection of masonry shear walls using fibre reinforced polymer strengthening." PhD thesis, University of Newcastle, Australia.

[4] Knox, C. L., Dizhur, D., & Ingham, J. M. (2016). Experimental Cyclic Testing of URM Pier-Spandrel Substructures. Journal of Structural Engineering, 04016177.

[5] Allen, C., Masia, M. J., Page, A. W., Griffith, M. C., Derakhshan, H., Mojsilovic, N. (2016). "Experimental testing of unreinforced masonry walls with openings subject to cyclic in-plane shear." Proc., 16th International Brick and Block Masonry Conference, Padova, Italy, on USB.

[6] Standards Australia. (2011). AS 3700: Masonry structures. Homebush, Australia.

[7] Standards Australia. (2003). AS/NZS 4456.15: Masonry units and segmental pavers and flags - Methods of test - Determining lateral modulus of rupture. Homebush, Australia.

[8] UNI EN. (2002). EN 1052-3. Methods of test for masonry. Part 3: Determination of initial shear strength. Brussels, Belgium.

[9] TNO DIANA (2012). DIANA Finite Element Analysis User's Manual Release 9.4.4. Delft, Netherlands.

[10] Lourenço, P. B. (1996). A user/programmer guide for the micromodeling of masonry structures. Report, 3(1.31), 35. Delft University of Technology, Netherlands.

[11] Lourenço, P. B. (2008). Structural masonry analysis: recent developments and prospects. Proc. 14th international brick and block masonry conference. University of Newcastle, Australia.

[12] Magenes, G., & Calvi, G. M. (1997). In-plane seismic response of brick masonry walls. Earthquake engineering & structural dynamics, 26(11), 1091-1112.